

Exploration of structural, optical, and photoluminescent properties of (1-*x*)$NiCo_2O_4$/*x*PbS nanocomposites for optoelectronic applications

Zein K Heiba, Mohamed Bakr Mohamed, Noura M Farag, and Ali Badawi

Citation: Chin. Phys. B, 2022, 31 (**6**): 067801. DOI: 10.1088/1674-1056/ac4235
Journal homepage: http://cpb.iphy.ac.cn; http://iopscience.iop.org/cpb

What follows is a list of articles you may be interested in

Effects of filler loading and surface modification on electrical and thermal properties of epoxy/montmorillonite composite

Zi-Rui Jia(贾梓睿), Zhen-Guo Gao(高振国), Di Lan(兰笛), Yong-Hong Cheng(成永红), Guang-Lei Wu(吴广磊), Hong-Jing Wu(吴宏景)

Chin. Phys. B, 2018, 27 (**11**): 117806. DOI: 10.1088/1674-1056/27/11/117806

Magnetic field aligned orderly arrangement of Fe_3O_4 nanoparticles in CS/PVA/Fe_3O_4 membranes

Meng Du(杜萌), Xing-Zhong Cao(曹兴忠), Rui Xia(夏锐), Zhong-Po Zhou(周忠坡), Shuo-Xue Jin(靳硕学), Bao-Yi Wang(王宝义)

Chin. Phys. B, 2018, 27 (**2**): 027805. DOI: 10.1088/1674-1056/27/2/027805

In-situ SAXS study on PET/ PMMT composites during tensile tests

Wei-Dong Cheng(程伟东), Xiao-Hua Gu(顾晓华), Xue Song(宋雪), Peng Zeng(曾鹏), Zhao-Jun Wu(吴昭君), Xue-Qing Xing(邢雪青), Guang Mo(默广), Zhong-Hua Wu(吴忠华)

Chin. Phys. B, 2016, 25 (**1**): 017802. DOI: 10.1088/1674-1056/25/1/017802

Synthesis and microwave absorption properties of graphene-oxide(GO)/polyaniline nanocomposite with gold nanoparticles

Fu Chen, He Da-Wei, WangYong-Sheng, Fu Ming, Geng Xin, Zhuo Zu-Liang

Chin. Phys. B, 2015, 24 (**8**): 087801. DOI: 10.1088/1674-1056/24/8/087801

Synthesis and microwave absorption properties of graphene-oxide(GO)/polyaniline nanocomposite with Fe_3O_4 particles

Geng Xin, He Da-Wei, Wang Yong-Sheng, Zhao Wen, Zhou Yi-Kang, Li Shu-Lei

Chin. Phys. B, 2015, 24 (**2**): 027803. DOI: 10.1088/1674-1056/24/2/027803

Exploration of structural, optical, and photoluminescent properties of $(1-x)NiCo_2O_4/xPbS$ nanocomposites for optoelectronic applications

Zein K Heiba[1,†], Mohamed Bakr Mohamed[1,2], Noura M Farag[1], and Ali Badawi[3,4,‡]

[1] *Physics Department, Faculty of Science, Ain Shams University, Cairo, Egypt*
[2] *Physics Department, Faculty of Science, Taibah University, Al-Madina al Munawarah, Saudi Arabia*
[3] *Department of Physics, College of Science, Taif University, P. O. Box* 11099, *Taif* 21944, *Saudi Arabia*
[4] *Department of Physics, University College of Turabah, Taif University, P. O. Box* 11099, *Taif* 21944, *Saudi Arabia*

(Received 13 November 2021; revised manuscript received 8 December 2021; accepted manuscript online 15 December 2021)

The $(1-x)NiCo_2O_4/xPbS$ ($0 \le x \le 0.2$) nanocomposite samples are synthesized using the hydrothermal and thermolysis procedures. The different phases developed in the obtained nanocomposite samples are accurately determined using the x-ray diffraction technique equipped with a line-detector. The percentage of the formed phases ($NiCo_2O_4$ (NCO), PbS, $PbSO_4$), structural and microstructure parameters are determined using Rietveld quantitative phase analysis. The transmission electron microscope (TEM) images and Rietveld analysis reveal almost isotropic particle size in the nano range with a very narrow size distribution. The obtained phase percentage of PbS and $PbSO_4$ are smaller than nominated values (x) suggesting dissolving of some Pb and S ions into NCO which is then confirmed by the analysis of Fourier-transform infrared (FTIR) spectra of nanocomposite samples. The absorption spectra are modified upon doping NCO with PbS. The optical band gaps of the nanocomposites increase as the amount of PbS augments. The effect of alloying on extinction coefficient, refractive index, dielectric constant, optical conductivity, the intensity, and emitted color from the photoluminescence of the nanocomposite samples are also studied. The refractive index value of NCO and NCO–PbS nanocomposite samples exhibit normal dispersions. The photoluminescent measurements reveal that the NCO–PbS nanocomposites can emit a violet color. The improvement in the values of the nonlinear optical (NLO) parameters of pristine NCO at high frequencies or the nanocomposite samples at low frequencies, are made them used in NLO photonic devices.

Keywords: $NiCo_2O_4$ and PbS, nanocomposite, FTIR, optical, photoluminescence

PACS: 78.67.Sc, 74.25.Gz, 78.55.–m, 77.84.Bw **DOI:** 10.1088/1674-1056/ac4235

1. Introduction

The rapid progress of nanocomposites materials enables a high degree of control over their optical and electronic characteristics.[1] The $NiCo_2O_4$ (nickel cobaltite; NCO) is of a mixed metal oxide spinel type, where nickel atoms occupy the octahedral sites while cobalt ones distribute over both octahedral and tetrahedral sites.[2] The NCO has attractive features such as low cost, low toxicity, eco-environmentally and natural abundance.[2] Lead sulfide (PbS) is a member of IV–VI group chalcogenide semiconductors has optical and optoelectronic characteristics made it able to be used in solar cells, optoelectronic devices, photoconductors, sensors, and infrared detector devices applications.[3] Nanocomposites of different oxides and/or sulfides reveal the interesting characteristics as compared with those of parent compounds. For instant, the 304 stainless steel was protected upon being coated by MnS/TiO_2 nanotube films under simulated solar light.[4] The $0.2ZnMn_2O_4/0.8ZnFe_2O_4$ nanocomposite sample revealed a good nonlinear optical behavior at low frequency.[5] The $CuCoO_x/BiVO_4$ multifunctional catalyst was applied to the organics' degradation, water oxidation and O_2 reduction under visible light.[6] Moreover, $NiO/NiCo_2O_4$ tubular structures with surface microporosity could have various applications such as the catalytic oxidation of harmful gases.[7] For $(1-x)CuCo_2O_4$-xCuS nanocomposites, the absorption spectrum of $x = 0.1$ sample displays a plateau in the visible region, that has a constant value in comparison with those of other composite samples.[8] The $Ni/NiCo_2O_4$ nanocomposite displayed a high nonlinearity and has tailorable linear and nonlinear optical features, which is beneficial to device applications.[9] The improvement in the electrical characteristics together with a reduction in the optical band gap of CeO_2 combined with PbS makes the resulting nanocomposite suitable for the solar cell uses.[10] The NCO@ZrO_2 exhibited an excellent performance in solar thermochemical procedure.[11] Ullah *et al*. demonstrated that the coupling of PbS with TiO_2 extended their photo response to visible range.[12] Adding PbS to MoS_2 adapted its fast response to the speed of mechanical exfoliation in detecting NO_2.[13] The intercalation of PbS into the layered space of $K_2La_2Ti_3O_{10}$ greatly enhanced the absorption edge and the photocatalytic activity.[14]

In the present study, the $(1-x)NiCo_2O_4/xPbS$ ($x = 0$, 0.1, 0.15, 0.2) nanocomposite samples are synthesized by the hydrothermal method and the thermolysis method. The effect of alloying NCO and PbS phases in a heterostructure nanocomposite matrix on the structure, optical, and photoluminescent characteristics are studied in detail using x-ray diffraction, Fourier-transform infrared spectroscopy, transmission electron

†Corresponding author. E-mail: zein_kh@yahoo.com
‡Corresponding author. E-mail: daraghmeh@tu.edu.sa

© 2022 Chinese Physical Society and IOP Publishing Ltd

microscope, photoluminescence, and UV-diffused absorption techniques.

2. Methods and materials

Nano $NiCo_2O_4$ sample was synthesized by dissolving a stoichiometric ratio of (nickel and cobalt) nitrates and urea in deionized water (35 ml) under magnetic stirring for 30 min. Then the solution was transferred into a teflon-lined stainless-steel autoclave and heated at 120 °C for one day. The autoclave allowed the solution to be cooled down to a room temperature. The formed solution was centrifuged and washed many times using deionized water and ethanol. The resulting powder was dried and annealed in an electric oven at 350 °C for 2 h (see Fig. 1(a)). To synthesize the $(1-x)NiCo_2O_4/x$PbS ($x = 0$, 0.1, 0.15, 0.2), the first step was to dissolve a stoichiometric ratio (1:1) of lead acetate and thiourea in 10 ml of deionized water in the presence the desired amount (x) of nano $NiCo_2O_4$ sample. The solution was stirred in a magnetic stirrer for 0.5 h then annealed at 250 °C for 2 h to avoid oxidizing the PbS (see Fig. 1(b)). All produced samples were explored by the techniques mentioned in Table 1. Tauc's and Beer–Lambert's formulas were used to find the direct optical bandgap[15]

$$\alpha h\nu = B(h\nu - E_g)^{0.5}, \tag{1}$$

$$\alpha = 2.303A/d, \tag{2}$$

$$\alpha = B(hc)^{n-1}\lambda\left(\frac{1}{\lambda} - \frac{1}{\lambda_g}\right), \tag{3}$$

$$A(\lambda) = D_1\lambda\left(\frac{1}{\lambda} - \frac{1}{\lambda_g}\right)^n + D_2. \tag{4}$$

The extinction coefficient (k), refractive index (n), real (ε_r), and imaginary (ε_i) dielectric constant, the optical conductivities (σ_{opt}), the third-order nonlinear optical susceptibility (χ^3), and the nonlinear refractive (n_2) can be obtained from Ref. [16] and shown as follows:

$$k = \lambda\alpha/4\pi, \tag{5}$$

$$n = \frac{(R+1) \pm \sqrt{3R^2 + 10R - 3}}{2(R-1)}, \tag{6}$$

$$\varepsilon_r = n^2 - k^2, \tag{7}$$

$$\varepsilon_i = 2nk, \tag{8}$$

$$\sigma_{opt} = \alpha nc/4\pi, \tag{9}$$

$$\chi^3 = 1.7 \times 10^{-10}\left(\frac{E_0E_g}{4\pi(E_0^2 - (h\nu)^2)}\right)^4, \tag{10}$$

$$n_2 = (12\pi/n)\chi^3, \tag{11}$$

where A, d, E_g, B, $h\nu$, λ_g, h, c, ($D_1 = [B(hc)^{n-1}d/2.303]$, D_2), λ, and R are the absorbance, thickness, optical band gap, constant, incident photon energy, the wavelength related to the optical gap, Planck's constant, light velocity, constants represent the reflection, the wavelength, and the reflectance, respectively.

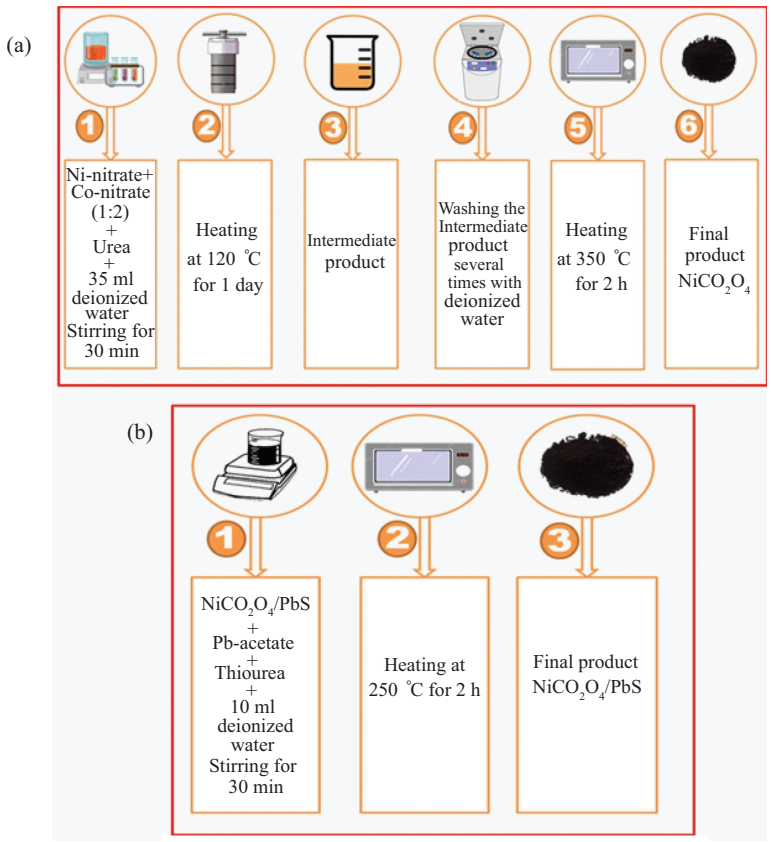


Fig. 1. The schematic diagram of formation of (a) $NiCo_2O_4$ and (b) $NiCo_2O_4$/PbS samples.

Table 1. List of investigation techniques.

Investigation technique	Devices and conditions
X-ray diffraction (XRD)	PANalytical diffractometer, copper source, LaB_6 standard for instrumental correction
High-resolution transmission electron microscope (TEM)	JEOL JEM-2100, 200 keV
Fourier-transform infrared spectroscopy (FTIR)	FTIR spectrometer (Bruker Tensor 27)
UV diffuse reflectance	Double-beam spectrophotometer (Shimadzu UV-VIS-2600) with attached integrating sphere assembly
Photoluminescence spectrofluorometer	Jasco FP-6500, Japan, Xenon lamb, 150 Watt

3. Results and discussion

3.1. Structural analysis

Using a line-detector, high quality x-ray diffraction (XRD) patterns have been recorded for the nanocomposite samples $(1-x)NiCo_2O_4/xPbS$ ($x = 0$, 0.1, 0.15, and 0.2) and depicted in Fig. 2(a). Accurate phase identification, using search-match program X'Pert HighScore Plus, can be performed due to the high quality of the diffraction patterns. Rietveld quantitative phase analysis[17] sreveals a single cubic spinel phase for the pristine $NiCo_2O_4$ ($x = 0.0$), while for composites $x = 0.1$, 0.15, and 0.2 three phases are identified: cubic spinel $NiCo_2O_4$ as a major phase ($> 95\%$), PbS, and $PbSO_4$ as minor phases. Table 2 lists the resulting structural and microstructure parameters obtained from Rietveld analysis and figure 2(b) shows the resulting diffraction pattern fitting. To determine the crystallite size of the minor phases, first the size is constrained within the size of the major phase NCO, then in subsequent final refinement the size parameter is freely refined. From Table 2 it may follow that the phase percentages of PbS and $PbSO_4$ are less than composition parameter (x) used for preparation which suggests the incorporation of some Pb and S ions into the $NiCo_2O_4$ lattice. The suggestion may be confirmed by the slight increase in the $NiCo_2O_4$ cell parameter due to the insertion of Pb ions which are larger than that of Ni or Co ones. The crystallite size of the $NiCo_2O_4$ phase is isotropic and almost the same (≈ 15 nm) for all samples (see Table 2). For $PbSO_4$ phase, the crystallite size is ≈ 17 nm while the PbS phase is large as given in Table 2. The TEM images given in Fig. 3 show very uniform particle morphology throughout the sample and good crystallinity. The particle size is almost isotropic with a very narrow size distribution as indicated by Rietveld analysis.

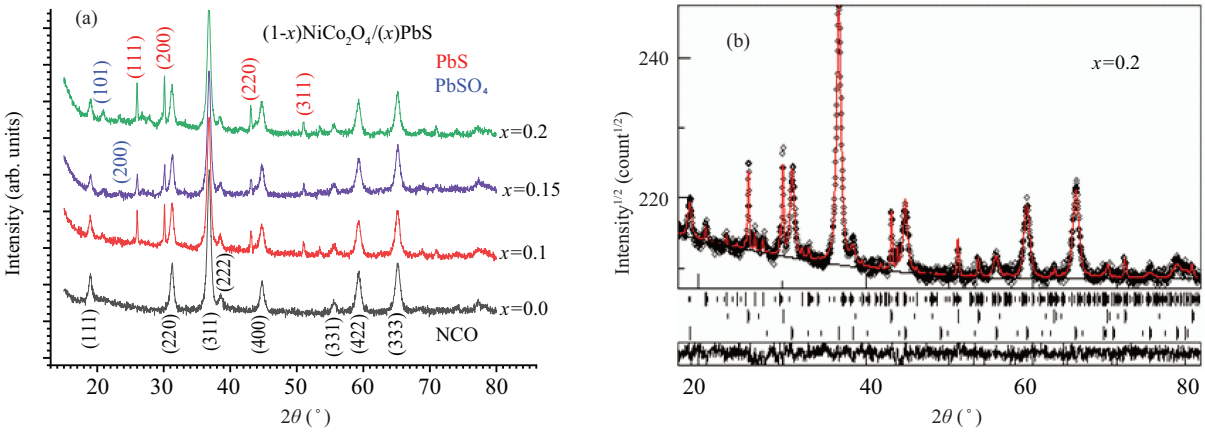


Fig. 2. (a) The x-ray diffraction patterns for $(1-x)NiCo_2O_4/xPbS$ sampls and (b) Rietveld refinement for $0.8NiCo_2O_4/0.2$ PbS sample.

Table 2. Cell parameters (in unit Å), crystallite size (in unit nm), and phase percentage (%) for $(1-x)NiCo_2O_4$–xPbS samples for different values of x.

x	$NiCo_2O_4$			PbS			$PbSO_4$				
	Size (Å)	a (Å)	%	Size (Å)	a (Å)	%	Size (Å)	a (Å)	b (Å)	c (Å)	%
0.0	14.1	8.0989(4)	100	–	–	–		–	–	–	–
0.1	15.2	8.0999	97.3	143	5.933(1)	2.0	17.2	8.488	5.397	6.961	0.7
0.15	16.1	8.1007	95.4	116	5.935	2.8	17.1	8.462	5.392	6.954	1.8
0.2	16.3	8.0992	95.2	125	5.935	2.9	17.1	8.460(1)	5.390	6.953	1.9

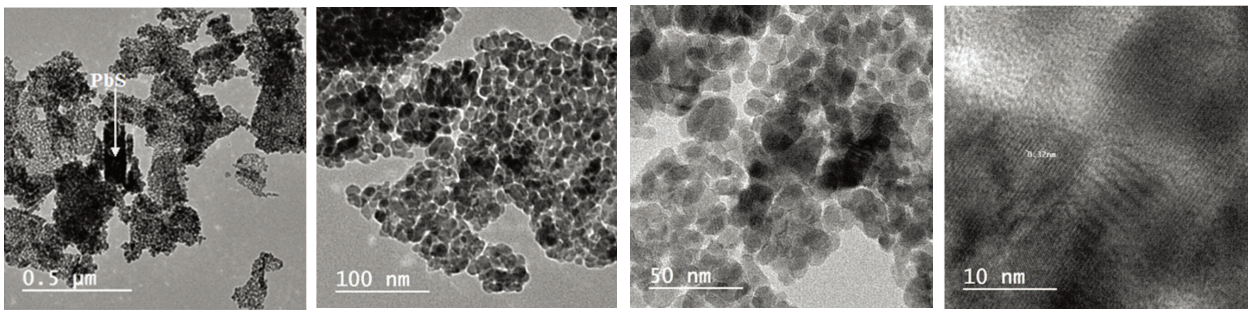


Fig. 3. TEM images with different magnifications for $0.8NiCo_2O_4/0.2PbS$ sample.

Infrared spectroscopy is used as an effective tool for investigating the local structure of transition metal oxides.[18] The measured Fourier-transform infrared (FTIR) spectra for the $(1-x)$NCO/xPbS nanocomposites are given in Fig. 4. There exist two sharp vibrational modes at 545.9 cm^{-1} and 648.9 cm^{-1} which can be assigned to primarily motion of the octahedral and tetrahedral metal–O, respectively.[18–20] For the composite samples ($x = 0.1$, 0.15, 0.2), the spectra contain two extra weak peaks observed around 1034 cm^{-1} and 1160 cm^{-1} which are characteristic peaks of the heteropolar diatomic molecules of Pb–S band.[21–23] Because the bond of Pb–S is mainly an electrovalent bond, the FTIR spectra of the samples do not show strong bands associated with Pb–S stretching nor those with bending vibrations.

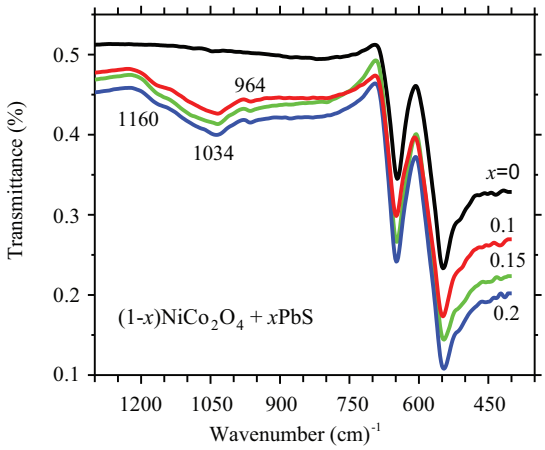


Fig. 4. The FTIR spectra for $(1-x)NiCo_2O_4/x$PbS samples.

3.2. Optical properties

The diffused absorption data for $(1-x)$NCO/xPbS nanocomposite samples are displayed in Fig. 5. As revealed from the graph, NCO sample exhibits a substantial amount of absorption in a range of 400 nm–800 nm similar to the absorption amount of $CoMn_2O_4$ sample.[24] This observation reveals the importance of this sample in visible light driven catalyst. The wide absorption of NCO sample may be caused by the absorption of the surface plasmons of nanoparticle and coupling of plasmon modes of the neighboring particle.[25] The absorption spectrum is modified due to NCO doped with PbS. The absorbance of NCO/xPbS nanocomposites decreases in the UV range while it increases in the visible range as compared with NCO as shown in Fig. 5(a). This behavior indicates that the absorption of the $(1-x)$NCO/xPbS nanocomposite is affected due to the presence of PbS in the sample. In contrary to the NCO@ZrO_2 composite, the NCO is predominant as reported in Ref. [11]. Furthermore, the absorption slightly increases as the amount of PbS and $PbSO_4$ phases increase in the nanocomposite matrix (see Table 2).

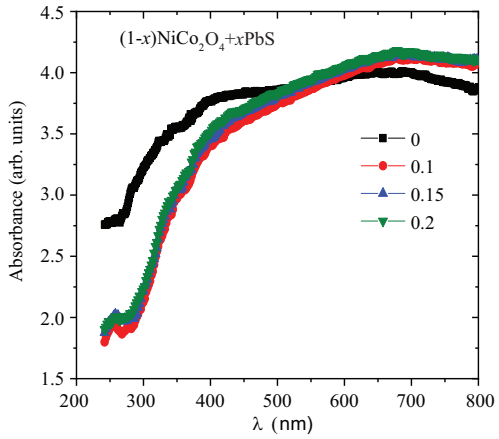


Fig. 5. Curves of UV-diffused absorbance spectra *versus* wavelength for $(1-x)NiCo_2O_4/x$PbS samples.

The values of direct optical band gap (E_g) for different samples are obtained from extrapolating the linear part of the plots between $(\alpha h\nu)^2$ *versus* $h\nu$ to zero absorption (see Fig. 6). As revealed from the graph, NCO has two band gaps of 1.35 eV and 2.33 eV which are in agreement with the values in Ref. [26]. These two energy gaps are ascribed to the electron movement from the O-2p valence band to the transition metals-3d (t_{2g}, e_g) conduction bands.[27] Furthermore, the two bands are attributed to the presence of high spin and low spin sates of Co^3 in the NCO sample.[27] As the NCO alloyed with PbS, the optical band gap increases to (3.3 eV, 4.06 eV), (3.33 eV, 4.1 eV), and (3.27 eV, 4.15 eV) as the amount of PbS becomes 10%, 15%, and 20%, respectively. The optical band gap of ZnO increases as the amount of Pb doping augments.[28] As indicated from XRD analysis in Table 2, the nanocomposite contain PbS and $PbSO_4$ beside the main phase of NCO. In addition, some Pb and S atoms are introduced into

NCO lattice as indicated by XRD results. All these variables affect the values of the optical energy gaps.

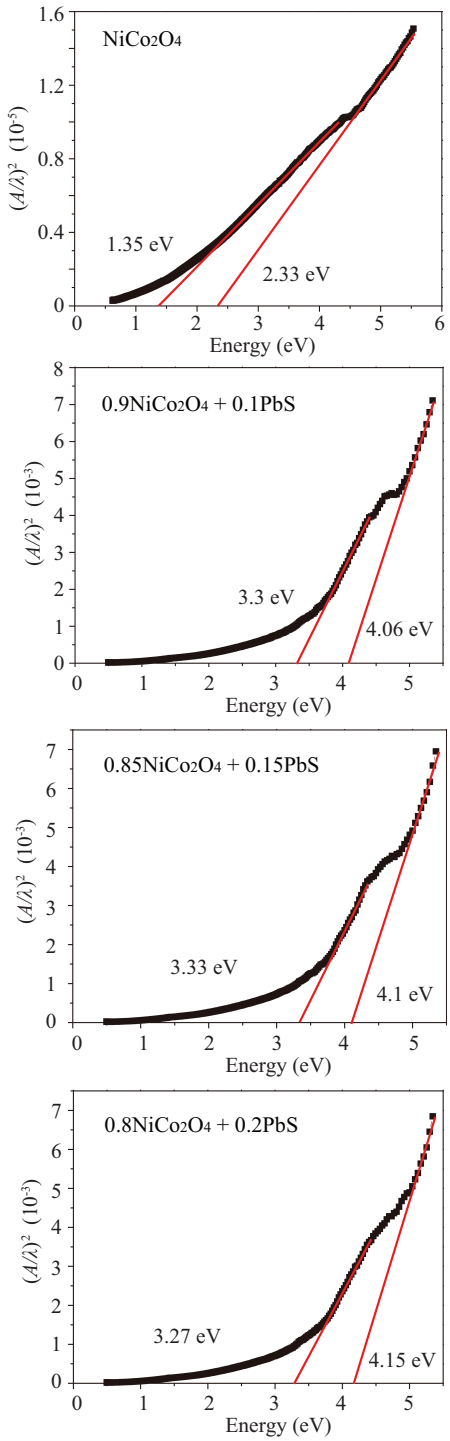


Fig. 6. The relation between $(A/\lambda)^2$ *versus* photon energy for $(1-x)$-$NiCo_2O_4/x$-PbS samples.

The refractive index n and absorption index k, related to refraction and absorption, respectively, rely on the interference between the samples under investigation and incident light: n is related to the phase velocity and associated with the dispersion, while k is linked to the coefficient of mass reduction and allows the determining of dissipation rate of the electromagnetic wave in the medium. The changing of the extinction coefficient (k) with the wavelength (λ) for $(1-x)$NCO/xPbS nanocomposite samples is displayed in Fig. 7.

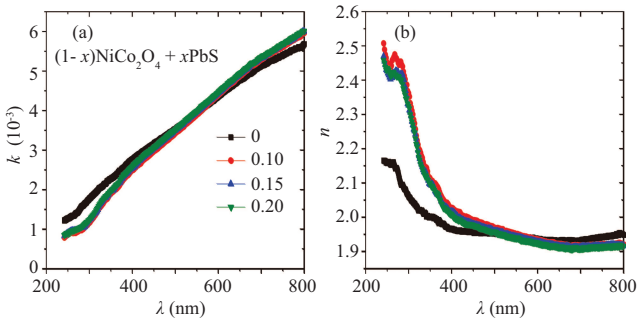


Fig. 7. Variations of (a) extinction coefficient and (b) refractive index with wavelength for $(1-x)NiCo_2O_4/x$PbS samples.

In the case of NCO sample, k increases as the wavelength augments, and so does the scenario in the $(1-x)$NCO/xPbS nanocomposite samples. In addition, as the percentage of PbS increases in the nanocomposite samples, the k values decrease at the lower wavelengths while they increase at higher wavelengths. The enhancement or decrease in k value may be linked to the strengthening or weakening of the absorption process depending on whether the excess free carriers exists or not.[29] The variation of the refractive index (n) with the wavelength for the $(1-x)$NCO/xPbS nanocomposite samples is shown in Fig. 7(b). The n value for the NCO and $(1-x)$NCO/xPbS nanocomposite samples decrease as the wavelength is increased. Therefore, the n values in all samples describe the degrees of the normal dispersion. Furthermore, the n value in the nanocomposite sample is higher than that of NCO sample; the situation is reversed in a higher wavelength range. In addition, as the content of PbS increases in the nanocomposite sample, the n value decreases slightly. The difference of value of n among different samples may be caused by the variations in the polarizability of the samples.[30] The variations in the real part (ε_r) and imaginary part (ε_i) of the dielectric constant and the optical conductivity (σ_{opt}) for $(1-x)$NCO/xPbS nanocomposite samples are shown in Fig. 8. Both ε_r and ε_i curves exhibit similar manners to the n and k curves, respectively for the corresponding samples. The value of ε_r decreases while the values of ε_i and σ_{opt} increase as the wavelength augments for each of all samples. Also, the values of ε_r of the nanocomposite samples in a lower wavelength range are higher than those of NCO samples. The values of ε_i and σ_{opt} of the nanocomposite samples in a lower wavelength range are lower than those of NCO samples. In a higher wavelength range, the behaviors of ε_r, ε_i, and σ_{opt} in the nanocomposite samples are reversed as compared with those of the NCO samples. The values of ε_r, ε_i, and σ_{opt} increase slightly as the amount of PbS increases in nanocomposite matrix. The variations of the values of ε_r and σ_{opt} are linked to the changing of the density of the localized states in

an optical bandgap of the host material and the ε_i varies with the modification of the dipole movement.[31]

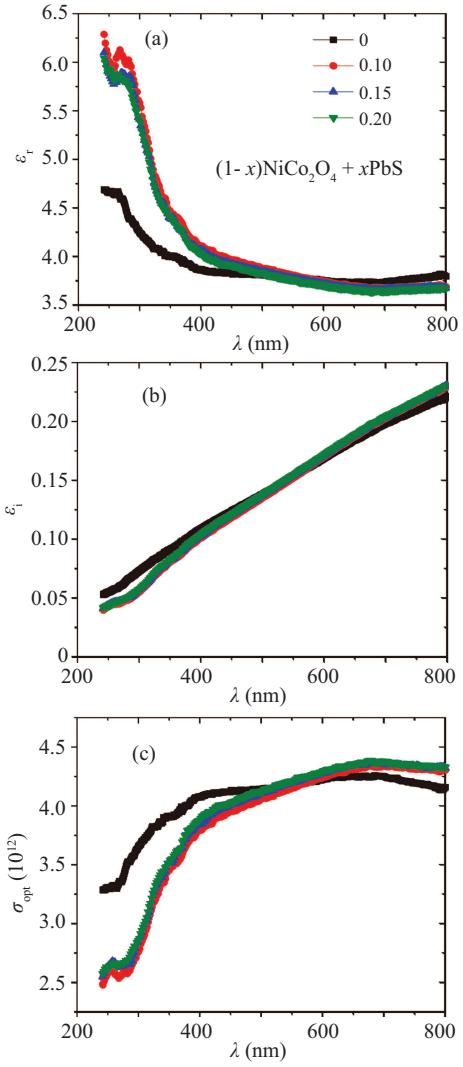


Fig. 8. Variations of (a) real part (ε_r) and (b) imaginary part (ε_i) of dielectric constant, and (c) curves of optical conductivity *versus* wavelength for $(1-x)NiCo_2O_4/x$PbS samples.

The nonlinear optical (NLO) characteristics such as χ^1 and n_2 play a crucial role in realizing the high performance communication networks devices. The values of χ^1, χ^3, and n_2 are dependent on the wavelength λ for all nanocomposite samples and shown in Fig. 9. The three parameters vary in a similar way, where the three parameters decrease with λ increasing in NCO and nanocomposite samples. The values of χ^1, χ^3, and n_2 values of the nanocomposite samples are higher than those of NCO samples. In addition, the values of χ^1, χ^3, and n_2 decrease slightly as the percentage of PbS increase in the nanocomposite matrix. The changing in the nonlinear parameters may be due to the variation in the number of defect centers and hence the changing in the local polarizabilities present in the different samples. The improvement in the values of χ^3 and n_2 in the nanocomposite samples makes the samples deserve to further studied so as to be used in numerous NLO and future photonic applications depending on the frequency range.

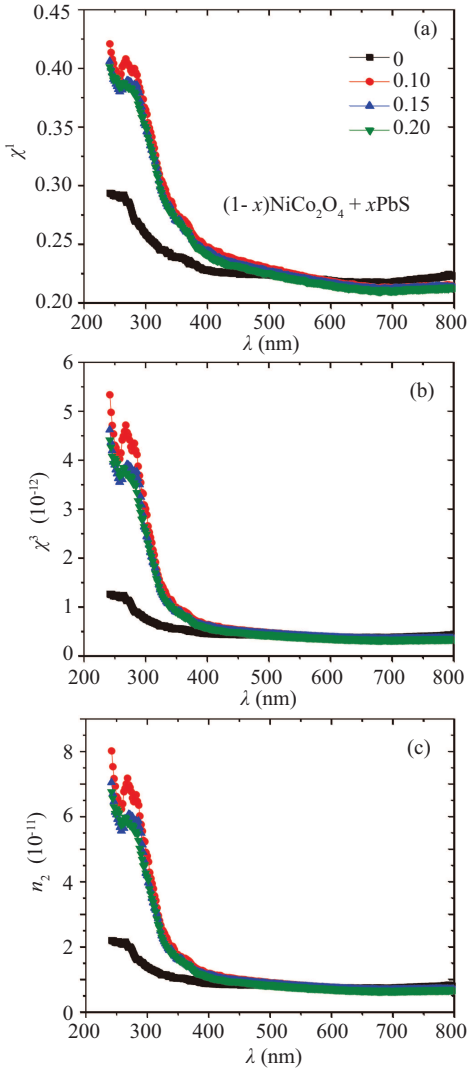


Fig. 9. Curves of wavelength dependent (a) χ^1, (b) χ^3, and (c) n_2 for $(1-x)NiCo_2O_4/x$PbS samples.

3.3. Photoluminescence analysis

Figure 10(a) shows the photoluminescence (PL) spectra emitted from $(1-x)$NCO/xPbS ($x = 0.0$, 0.1, 0.15, and 0.2) system under an exciting λ of 300 nm at room temperature. The PL intensity increases as the amount of PbS becomes 10% and 15% in the nanocomposite system relative to NCO sample, while it decreases as the content of PbS increases further in the matrix. The intensification or suppression in the luminescence intensity may be caused by the increasing or decreasing of the recombination rate between the photo-induced electrons (e^-) and holes (h^+) pairs which depends on the trap levels existent in the bandgaps of the different samples.[32] A similar result was observed in two-dimensional PbS/amorphous MoS_x heterojunction composites.[33] The enhancement and reduction in the PL intensity of the different samples may make these materials able to possess the LED and photocatalytic applications.

Using Gaussian function, the PL spectrum for each of all samples can be decomposed into ultraviolet color and violet colos (see Figs. 8(b)–8(e)). The direct recombination of the electrons via an exciton-exciton collision process produces the ultraviolet color and violet color.[34]

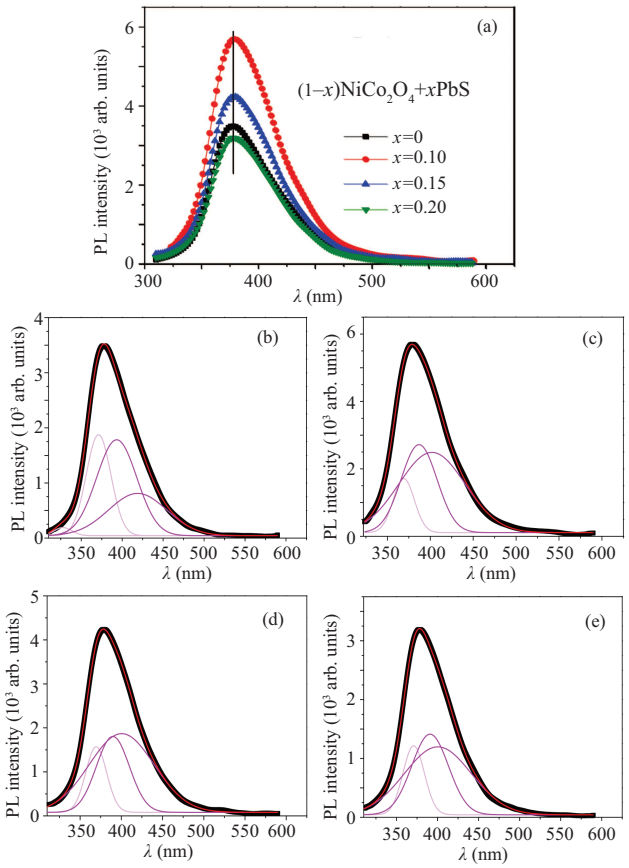


Fig. 10. (a) Photoluminescence measurements and [(b)–(e)] Gaussian fitting of photoluminescence measurements for $(1-x)NiCo_2O_4/x$PbS samples under 300 nm.

4. Conclusions

The pristine $NiCo_2O_4$ (NCO) has a single cubic spinel phase, while the $(1-x)$NCO/xPbS nanocomposite samples with $x = 0.1$, 0.15, and 0.2 have three phases: cubic spinel NCO as a major phase ($> 95\%$), PbS, and $PbSO_4$ as minor phases. Some Pb and S ions are incorporated into the NCO lattice. The cell parameter of NCO phase increases as the amount of PbS augments in the nanocomposite sample. The crystallite size of the NCO phase is isotropic and almost the same ($\approx$ 15 nm) for all samples. For the $PbSO_4$ phase, the crystallite size is $\approx$ 17 nm while for PbS phase it is very large ($\sim$ 130 nm). The FTIR spectra reveal the heteropolar diatomic molecules of Pb–S band existent in the nanocomposite's samples. The NCO sample exhibits a substantial amount of absorption in the visible light range. For the NCO alloyed with PbS, the absorption decreases in the UV range while it increases in the visible range. The NCO has two band gaps of 1.35 eV and 2.33 eV which increase to (3.3 eV, 4.06 eV), (3.33 eV, 4.1 eV), and (3.27 eV, 4.15 eV) upon increasing PbS to 10%, 15%, and 20%, respectively. In all samples, the values of n, ε_r, and the nonlinear optical behavior decrease while the values of k, ε_i, and σ_{opt} increase as the wavelength augments. For the PbS alloyed with NCO, the dielectric constant, optical conductivity, and the nonlinear optical parameters are enhanced as compared with counterparts for the NCO sample. As the percentage of PbS increases, the values of k, n, ε_r, ε_i, σ_{opt}, and NLO decrease slightly. The PL spectra for all samples can be decomposed into ultraviolet and violet colors. The enhancement and reduction in the PL intensity of the different samples may make these materials able to possess the LED and photocatalytic applications.

Acknowledgment

The authors thank the support of Taif University Researchers Supporting Project Number TURSP-2020/12, Taif University, Taif, Saudi Arabia.

References

[1] Heiba Z K, Mohamed M B, Farag N M and Ahmed S I 2021 *Appl. Phys. A* **127** 1
[2] Jin C, Lu F, Cao X, Yang Z and Yang R 2013 *J. Mater. Chem.* **1** 12170
[3] Ganeev R A, Shuklov I A, Zvyagin A I, Dyomkin D V, Bocharova S I, Popov V S, Toknova V F, Lizunova A A, Ovchinnikov O V and Razumov V F 2021 *Opt. Mater.* **121** 111499
[4] Ge S S, Zhang Q X, Wang X T, Li H, Zhang L and Wei Q Y 2015 *Surf. Coat. Technol.* **283** 172
[5] Heiba Z K, Mohamed M B, El-naggar A M and Altowairqi Y 2021 *Chem. Phys. Lett.* **784** 139110
[6] Chen M, Zhao J, Wang Y, Huang X and Xu Y 2021 *J. Hazard. Mater.* **419** 126515
[7] Kim Il H, Lee H, Yu A, Jeong J H, Lee Y, Kim M H, Lee C and Kim Y D 2018 *Nanotechnology* **29** 175702
[8] Heiba Z K, Deyab M A, Mohamed M B, Farag N M, El-naggar A M and Plaisier J R 2021 *Appl. Phys. A* **127** 1
[9] Rahulan K M, Padmanathan N, Philip R and Balamurugan S and Kanakam C C 2013 *Appl. Surf. Sci.* **282** 656
[10] Mohanty B, Chattopadhyay A and Nayak J 2021 *J. Alloys Compd.* **850** 156735
[11] Macias J D, Bacelis-Martinez R D, Ruiz-Gomez M A, Bante-Guerra J, Villafan-Vidales H Il, Rodriguez-Gattorno G, Romero-Paredes H and Alvarado-Gil J J 2021 *Int. J. Hydrog.* **46** 0632
[12] Ullah K, Meng Z D, Ye S, Zhu L and Oh W C 2014 *J. Ind. Eng. Chem.* **20** 1035
[13] Tan J, Hu J, Ren J, Peng J, Liu C, Song Y and Zhang Y 2020 *Chin. Chem. Lett.* **31** 2103
[14] Cui W, Qi Y, Liu L, Rana D, Hu J and Liang Y 2012 *Prog. Nat. Sci.* **22** 120
[15] Tauc 1972 *The Optical Properties of Solid*, Abeles A (Ed.) (Amsterdam: North Holland) p. 277
[16] Heiba Z K, Mohamed M B, Farag N M, El-naggar AM and Altowairqi Y 2021 *J. Mater. Sci.: Mater. Electron.* **32** 27121
[17] Rodríguez-Carvajal J 1993 *Physica B* **192** 55
[18] Zhang K, Zhen C, Wei W, Guo W, Tang G, Ma L, Houa D and Wu X 2017 *RSC Adv.* **7** 36026
[19] Jr C F W, Exarhos G J and Owings R R 2004 *J. Appl. Phys.* **95** 5435
[20] Roginskaya Y E, Morozova O V, Lubnin E N, Ulitina Y E, Lopukhova G V and Trasatti S 1997 *Langmuir* **13** 4621
[21] Zhao Y, Zou J and Shi W 2005 *Mater. Sci. Eng. B* **121** 20
[22] Suganya M and Balu A R 2017 *Mater. Sci. Poland* **35** 322
[23] Mozafari M, Moztarzadeh F and Tahriri M 2011 *Adv. Appl. Ceram.* **110** 30

[24] Vigneshwaran P, Kandiban M, Kumar N S, Venkatachalam V, Jayavel R and Potheher I V 2016 *J. Mater. Sci.: Mater. Electron.* **27** 4653
[25] Tharayil N J, Raveendran R and Vaidyan A V 2008 *Ind. J. Pure Appl. Phys.* **46** 47
[26] Umeshbabu E, Rajeshkhanna G, Justin P and Rao G R 2015 *Mater. Chem. Phys.* **165** 235
[27] Hu L, Wu L, Liao M Y, Hu X and Fang X S 2012 *Adv. Funct. Mater.* **22** 998
[28] Turgut G and Metall E 2014 *Mater. Trans. A* **45** 3675
[29] Dawood M S, Elmosalami T A and Desoky W M 2021 *Opt. Mater.* **117** 111101
[30] Mohamed S H and Drese R 2006 *Thin Solid Films* **513** 64
[31] Suma G R, Subramani N K, Shilpa K N, Sachhidananda S and Satyanarayana S V 2017 *J. Mater. Sci.: Mater. Electron.* **28** 10707
[32] Heiba Z K, Mohamed M B and Imam N G 2017 *J. Supercond. Nov. Magn.* **30** 3123
[33] Li M, Wang X, Ruan H, Zhang Q Wu, Z, Liu Y, Lu Z and Hai J 2018 *J. Alloys Compd.* **768** 399
[34] Rattana T, Suwanboon S, Amornpitoksuk P, Haidou A and Limsuwan P 2009 *J. Alloys Compd.* **480** 603